# Silicon quantum dot superstructures for all-silicon tandem solar cells

P. Löper[†‡], M. Künle[†], A. Hartel[†], J. C. Goldschmidt[†], M. Peters[†], S. Janz[†], M. Hermle[†], S. W. Glunz[†], M. Zacharias[‡]
[†] Fraunhofer Institute for Solar Energy Systems, Heidenhofstr. 2, 79110 Freiburg, Germany
[‡] IMTEK, University of Freiburg, Georges-Koehler-Allee 103, 79110 Germany
Phone: +49 (0) 761 4588 5475 Fax: + 49 (0) 761 4588 9250
Email: philipp.loeper@ise.fraunhofer.de

## Motivation

Silicon quantum dot absorber layers are used as building blocks for all-silicon tandem solar cells. A control of the Si nanocrystal size allows the adjustment of essential material parameters such as bandgap and oscillator strengths due to size quantization effects. This allows to fabricate silicon based top and middle cells with an engineered and optimized band gap for all-silicon tandem cells, increasing the theoretical efficiency limit of a silicon solar cell from 29 % to 42.5 % for two and 47.5 % for three cells [1]. In this paper, we present the optical and electrical characterization of Si quantum dots embedded in a dielectric SiC matrix for solar cell applications with special emphasis on the electrical transport through the superstructure and the reduction of recombination via defects at the interface between nanocrystals and the dielectric matrix. In order to build a photovoltaic device, both carrier transport properties and recombination properties have to be optimised by appropriate deposition, annealing and passivation procedures.

## Introduction

In our approach, a silicon quantum dot superstructure embedded in a silicon carbide matrix is used as the absorber layer [5]. The Si nanocrystal size and density control is achieved by the deposition and annealing conditions. Both single layers and multilayers are prepared in an AK-400 Plasma Enhanced Chemical Vapour Deposition (PECVD) reactor employing a high frequency source and a microwave source for plasma excitation. Silane ($SiH_4$) and methane ($CH_4$) and argon (Ar) are used as precursor gases [5]. After deposition a subsequent thermal annealing step is performed. The annealing temperature is varied to study the crystallisation behaviour and to optimise the material properties such as nanocrystal size, effective bandgap and carrier lifetime. In order to obtain a lower defect density, the annealed layers are passivated in a remote hydrogen plasma and in forming gas. The first step is to analyse how Si nanocrystals evolve by thermal annealing of Si rich SiC single layers. These single layers are being thoroughly investigated with respect to their structural, optical and electronic properties. The next step is the deposition and characterisation of multilayers consisting of the optimised single layers, following the multilayer approach introduced by Zacharias *et al.* [6]. The quantum dot absorber layers are characterized in each production stage (single and multi layers, as deposited, annealed at various temperatures and defect passivated) by UV-Vis spectroscopy, Fourier transformed infrared spectroscopy (FTIR) and glacing incidence x-ray diffraction (GIXRD). Please refer to the presentation of M. Künle (this conference) for details on the material preparation and analysis.

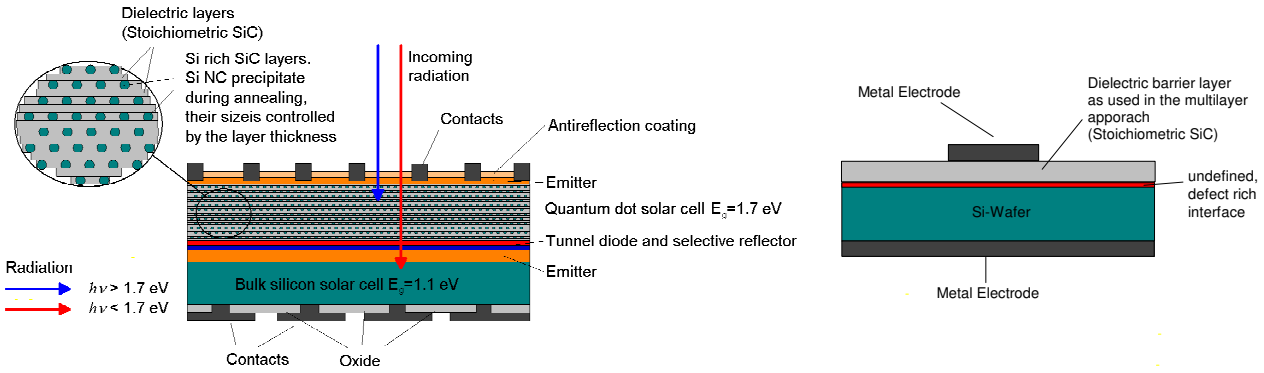


***Figure 1:*** *Principle of an all-silicon tandem cell with a quantum dot top solar cell (left). The control of the bandgap allows extending the concept to multi solar cells employing three or more cells. The bandgap is tuned by a size control of the Si nanocrystals employing the multilayer approach [6]. Recombination via interface defect states is a central issue for such a device. Metal Isulator Semiconductor (MIS) will be built to assess the properties of the interfaces (right), e.g. between the Si-and the SiC dielectric barrier and their temperature behaviour.*

**Experimental**

The optical bandgap $E_{g,\ optical}$ was obtained from the analysis following the procedure of Tauc [7] and correlates well with the energy of the PL maximum $E_{peak,\ PL}$ and $E_{04}$. $E_{04}$ is the photon energy at which the absorbance is $10^{-4}$ $cm^{-1}$. Photoluminescence (PL) measurements were performed under 514.5 nm excitation ($Ar^{+}$-Ion laser) and the luminescence was detected with a Si-CCD camera that was cooled by a combined thermoelectrical and water cooling to -100 °C. A longpass filter was used in the detection system to block the laser line. All measurements presented in this paper were done at room temperature. All spectra were corrected for the transmission function of the entire detection system. GIXRD was carried out with a Simens X'Pert MRD system employing $CuK_{\alpha}$ radiation at a wavelength of 1.54 A under an angle of incidence of 0.3°.

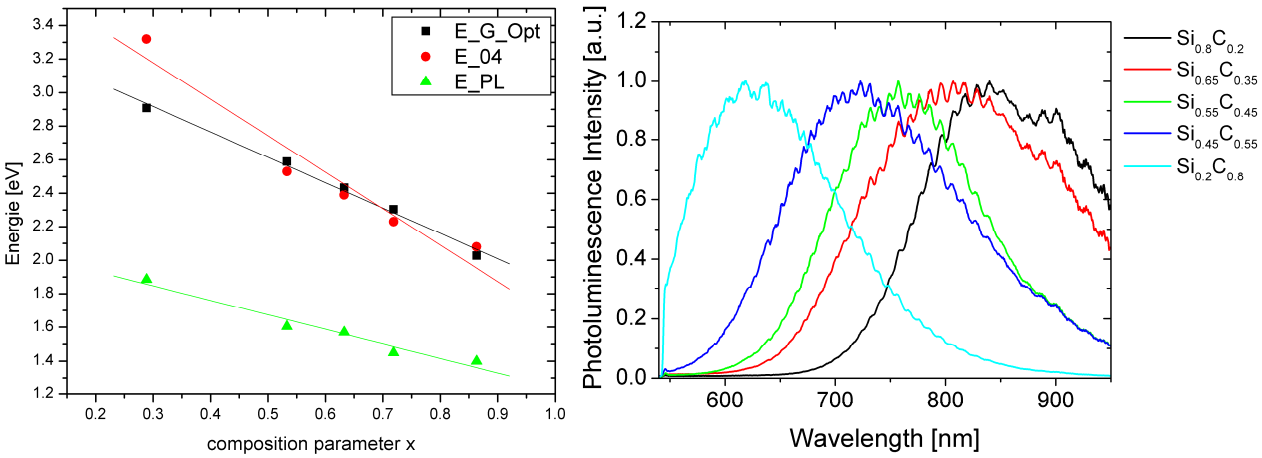


***Figure 2:*** *Evolution of the bandgap of the as deposited amorphous $Si_xC_{1-x}$:H layers (left). Right: Normalised photoluminescence of the as- deposited layers. A blue shift of the peak position with increasing carbon content is observed.*

**Results and Discussion**

The evolution of the bandgap of the as deposited amorphous $Si_xC_{1-x}$:H layers can be seen in Figure 2, left. The optical bandgap $E_{g,\ optical}$ was tuned between 2 and 2.9 eV by adjusting the silan and methan gas flows. Silicon rich carbide films with varying composition were annealed at 900°C and 1100°C. The photoluminescence of three samples with the compositions $Si_{0.8}C_{0.2}$, $Si_{0.65}C_{0.35}$ and $Si_{0.55}C_{0.45}$ is shown in Figure 3. After a 900°C anneal (Figure 3 left), the $Si_{0.55}C_{0.45}$-layer showed a weak PL signal with its peak at 600 nm, while the Si richer samples $Si_{0.65}C_{0.35}$ and $Si_{0.8}C_{0.2}$ do not emit detectable PL. After annealing at 1100°C, however, all layers show PL (Figure 3 right). The silicon richest sample shows the strongest PL signal. We observe a decrease of the PL intensity and a blueshift of the PL peak energy with increasing carbon content. The excitation wavelength of 514.5 nm is a limitation for this experiment, because the absorbance of the stoichiometric and carbon rich layers is low at this wavelength and transitions occur mainly between the band tails.

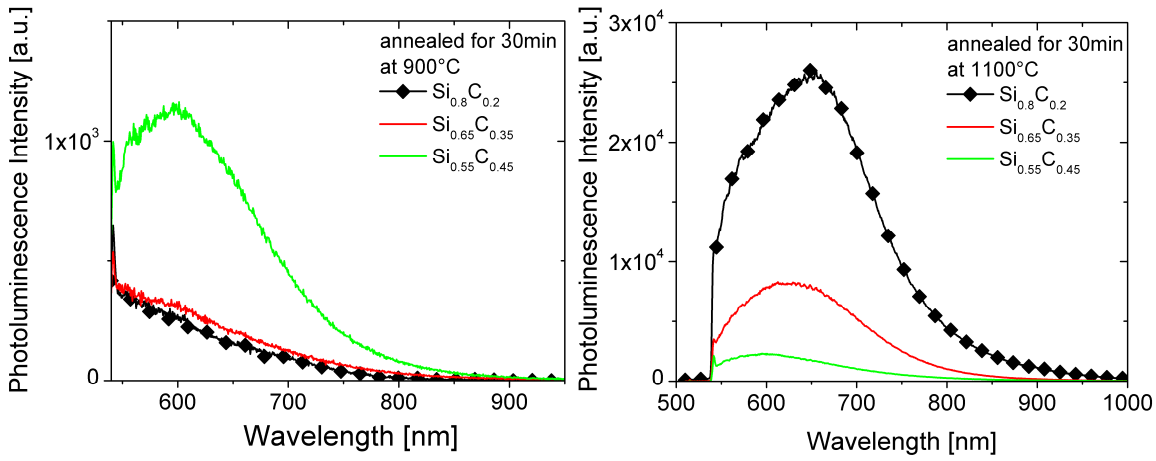


***Figure 3:*** *Photoluminescence of silicon rich SiC thin films with varying composition annealed at 900°C (left) and 1100°C (right).*

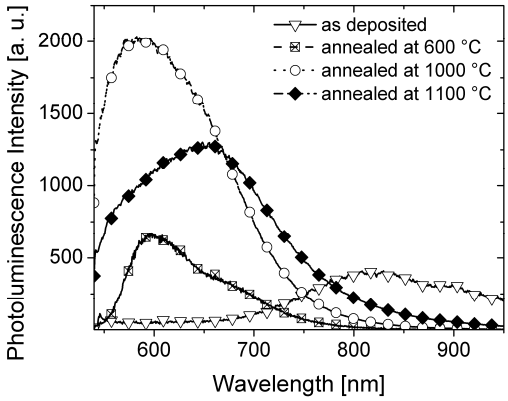


***Figure 4:*** *Photoluminescence for a series of different annealing temperatures of the sample $Si_{0.8}C_{0.2}$. Samples that were annealed at 1000 °C and 1100 °C show luminescence at 600 nm and 650 nm, respectively, and are blueshifted with respect to the PL of the as deposited (amorphous) sample.*

A series of different annealing temperatures was performed to investigate the crystallization behaviour of the sample $Si_{0.8}C_{0.2}$ (Figure 4). The samples were annealed under $N_2$ atmosphere between 500 °C and 1100 °C in incremental steps of 100 °C. The PL signal is quenched for annealing temperatures below 1000 °C with an exception at 600 °C. Samples that were annealed at 1000 °C and 1100 °C show luminescence at 600 nm and 650 nm, respectively, and are blueshifted with respect to the PL of the as deposited (amorphous) sample.

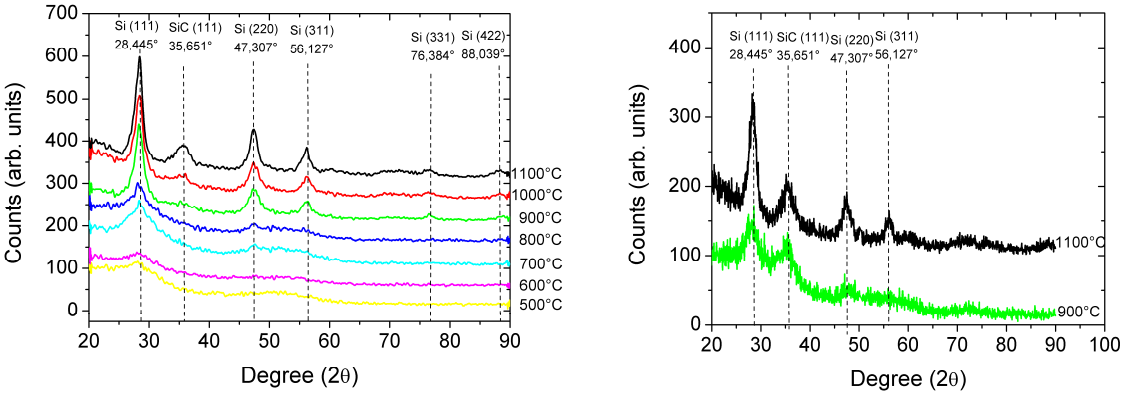


***Figure 5:*** *X-ray diffractogramms of the samples $Si_{0.8}C_{0.2}$ and $Si_{0.65}C_{0.35}$. In the sample with less silicon ($Si_{0.65}C_{0.35}$) apparently more SiC-nanocrystals are formed relative to Si nanocrystals.*

The formation of nanocrystals in the $Si_{0.8}C_{0.2}$ and the $Si_{0.65}C_{0.35}$ layers as a function of the annealing temperature was investigated by GIXRD as presented in Figure 5. In the silicon rich sample $Si_{0.8}C_{0.2}$ (Figure 5 left), silicon begins to agglomerate around 700 °C (broad peak at 28.445 °) and crystallises at temperatures of 900 °C and above. Additional to the formation of Si nanocrystals we observe SiC nanocrystals after annealing at 1100 °C. In the sample with less Si content ($Si_{0.65}C_{0.35}$, Figure 5 right) we observe both Si and SiC crystallites after a 900 °C anneal, and also after the 1100 °C anneal the SiC peak is more pronounced compared to the Si peak than in the Si richer $Si_{0.8}C_{0.2}$ sample. Apparently larger SiC-nanocrystals are formed relative to Si nanocrystals in the sample with less silicon ($Si_{0.65}C_{0.35}$).

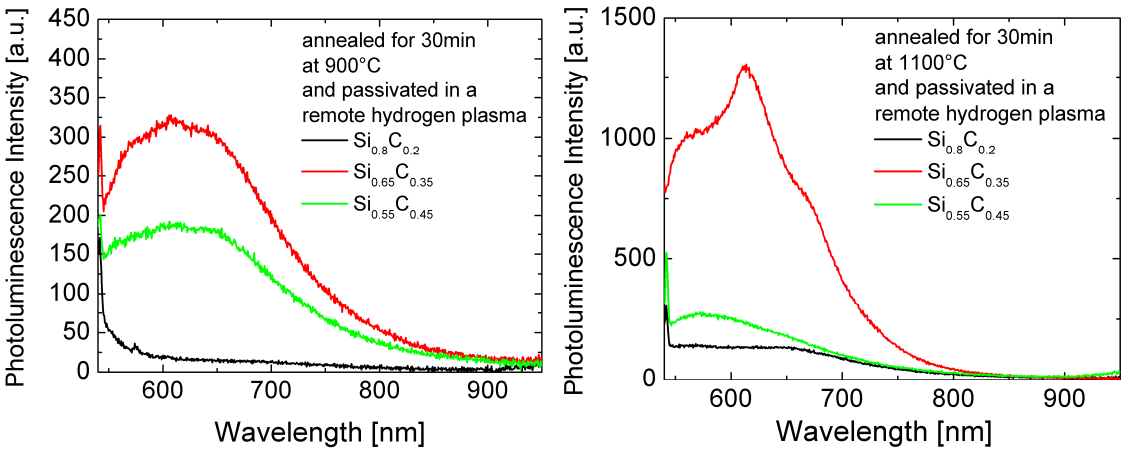


***Figure 6:*** *PL of the hydrogen passivated layers. Hydrogen passivation had the largest impact on the $Si_{0.65}C_{0.35}$ sample. Before passivation, no luminescence was detected in the 900°C sample, while after hydrogen passivation a clear peak is observable. The $Si_{0.65}C_{0.35}$ sample annealed at 1100 °C shows a change on the PL peak form.*

Si nanocrystals possess a huge surface compared to their crystalline volume and thus a large defect density. A crucial issue for Si nanocrystal absorber layers is the passivation of surface defects and a successful engineering of the interface properties. The annealed samples were treated by a remote hydrogen plasma in order to passivate dangling bonds in the SiC dielectric and at the interfaces between the Si nanocrystals and the surrounding SiC. Hydrogen passivation had the largest impact on the $Si_{0.65}C_{0.35}$ sample. Before passivation, no luminescence was detected in the 900°C sample, while after hydrogen passivation a clear peak is observable. The $Si_{0.65}C_{0.35}$ sample annealed at 1100 °C shows a change on the PL peak form.

**Conclusion**

Si nanocrystals incorporated in SiC single layers were fabricated and charaterised. The formation of Si nanocrystals begins to takes place at ~900 °C annealing temperature. During annealing at 1100 °C also SiC nanocrystal evolve. The formation of SiC nanocrystals seems to quench the PL signal. The silicon richest sample $Si_{0.8}C_{0.2}$ shows PL after annealing at 1000 °C which is still visible, after hydrogen passivation but lower than before passivation. This indicates that the PL signal before passivation is mainly due to defects but that after passivation the PL signal does not stem from defect luminescence but from the wanted transitions in the quantum dots. Therefore, this layer will be further investigated and optimised and then employed in the multilayer approach.

**References**

[1] M.A. Green, Third generation photovoltaics - advanced solar energy conversion, Vol. 12, Springer, Berlin, Heidelberg, New York, 2003.

[2] E.-C. Cho, M.A. Green, G. Conibeer, D. Song, Y.-H. Cho, G. Scardera, S. Huang, S. Park, X.J. Hao, Y. Huang, et al., Advances in OptoElectronics 2007 (2007) 1.

[3] D. Song, E.-C. Cho, G. Conibeer, C. Flynn, Y. Huang and M.A. Green, Solar Energy Materials & Solar Cells 92 (2008) 474.

[4] R. Rölver, B. Berghoff, D. Bätzner, B. Spangenberg, H. Kurz, M. Schmidt and B. Stegemann, Thin Solid Films (2008) in press.

[5] M. Kuenle, S. Janz, O. Eibl, C. Berthold, V. Presser and K.-G. Nickel, Material Science and Engineering B (2008).

[6] M. Zacharias, J. Heitmann, R. Scholz, U. Kahler, M. Schmidt and J. Bläsing, Applied Physics Letters 80 (2002) 661.

[7] J. Tauc and A. Menth, Journal of Non-Crystalline Solids 8 (1972) 569.